Tracking frequency laser distance gauge

J. D. Phillips[a] and R. D. Reasenberg
Smithsonian Astrophysical Observatory, Harvard-Smithsonian Center for Astrophysics, MS63, 60 Garden St., Cambridge, Massachusetts 02138

(Received 6 May 2004; accepted 14 February 2005; published online 17 May 2005)

Advanced astronomical missions with greatly enhanced resolution and physics missions of unprecedented accuracy will require laser distance gauges of substantially improved performance. We describe a laser gauge, based on Pound–Drever–Hall locking, in which the optical frequency is adjusted to maintain an interferometer's null condition. This technique has been demonstrated with pm performance. Automatic fringe hopping allows it to track arbitrary distance changes. The instrument is intrinsically free of the nm-scale cyclic bias present in traditional (heterodyne) high-precision laser gauges. The output is a radio frequency, readily measured to sufficient accuracy. The laser gauge has operated in a resonant cavity, which improves precision, can suppress the effects of misalignments, and makes possible precise automatic alignment. The measurement of absolute distance requires little or no additional hardware, and has also been demonstrated. The proof-of-concept version, based on a stabilized HeNe laser and operating on a 0.5 m path, has achieved 10 pm precision with 0.1 s integration time, and 0.1 mm absolute distance accuracy. This version has also followed substantial distance changes as fast as 16 mm/s. We show that, if the precision in optical frequency is a fixed fraction of the linewidth, both incremental and absolute distance precision are independent of the distance measured. We discuss systematic error sources, and present plans for a new version of the gauge based on semiconductor lasers and fiber-coupled components. [DOI: 10.1063/1.1921408]

I. INTRODUCTION

Metrology based on laser distance gauges will be an enabling technology for a new generation of astronomical missions characterized by large and distributed apertures and by unprecedented performance, spanning the spectrum from mm waves to x rays. These observatories will have demanding requirements for metrology,[1,2] which traditional laser gauge architectures have so far proved incapable of meeting. Precision laboratory measurements ranging from tests of the equivalence principle to gravity gradiometry, including space-based versions, will similarly benefit from substantially improved laser gauges. A new architecture is needed.

The quasistatic homodyne laser gauge using quadrature detection is normally limited in accuracy to no better than $\lambda/100$. The classical precision laser gauges employ two beams and a heterodyne principle. In the most common configuration, the beams are overlapped, transported together to the measurement interferometer, and separated there using a polarizing beamsplitter. One traverses the measurement path and the other traverses the reference path. They are recombined by a beamsplitter, and fall on a detector. Imperfect separation leads to nm-scale cyclic bias. Reduction of the bias by dithering and averaging over the cycle has led to improvements, but limits the maximum readout rate to $\sim$1 kHz.[3] The amplitude of this bias has been reduced to 10 pm, without averaging, using spatial separation of beams.[4–7] To enhance the separation of beams, at the cost of additional complexity, a combination of polarization and spatial separation has been used.[8] For the highest precision distance measurement, it would be desirable to operate in a resonant cavity and gain in precision by the finesse. Although heterodyne gauges do not function in a cavity, they can be operated in a multi-pass interferometer, thus achieving some of the advantages of a cavity, again at the expense of additional complexity.

The technique of locking a laser to a cavity and measuring the optical frequency by heterodyne against a stable laser has been used for measurement of refractive index.[9,10] The work here differs in that this technique is used to measure a distance that changes. For changes too great for the available frequency shift range (which is often no more than several wavelengths), the laser must hop from one fringe to another. We have demonstrated a tracking frequency laser gauge (TFG) that can hop as often as every 20 μs.

To measure absolute distance, we and others measure the difference of optical frequency of nearby interferometer orders. Stone *et al.*[11] report the difference of successive path measurements in a lab environment, as a function of the time between readings, τ. The range of τ is 0.05–10 s. They state that these differences are dominated by air turbulence, with an rms roughly proportional to $\tau^{1/2}$. The TFG can hop between interferometer orders at $>$1 kHz, so should realize a substantial reduction of absolute distance error due both to turbulence and to vibration.

In applications requiring the highest sensitivity, such as potential spaceborne tests of the equivalence principle, there can be a requirement that fluctuations in the pressure of the

[a]Author to whom correspondence should be addressed; electronic mail: jphillips@cfa.harvard.edu

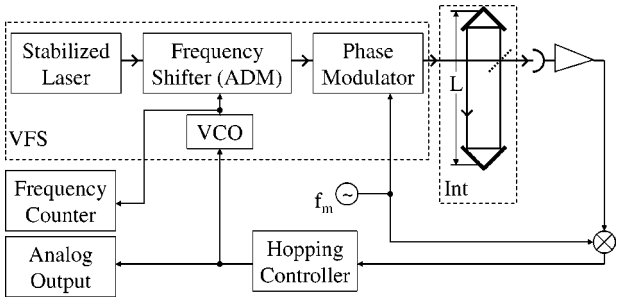

FIG. 1. Block diagram of the tracking frequency laser gauge (TFG) as currently implemented in a cavity. "Int" is the measurement interferometer whose length, L, is to be measured. Digital output is *via* frequency counter.

measuring light have a minimum impact on the system being measured. For a fixed measurement time, there is a power level that minimizes the sum of shot-noise-dominated measurement error and disturbance due to radiation pressure fluctuation. Caves[12,13] has investigated the effect of radiation pressure fluctuation on the sensitivity of a gravitational radiation detector based on a nonresonant interferometer, and Jacobs *et al.*[14] have extended this work to resonant optical cavities, including phase modulation detection. In this article, we do not further address either this issue or these very high accuracy applications.

In Sec. II, we discuss an alternative to the heterodyne approach, the TFG.[15,16] In Sec. III, we discuss the current implementation of the TFG and the results from tests of that version. Finally, in Sec. IV, we introduce a series of techniques that we plan to use as part of a more robust, capable, and potentially space-worthy laser gauge that we are developing, the semiconductor laser TFG (SL-TFG). In the Appendix, we show that measurement of absolute distance is based on group delay. Except for the analysis in the Appendix, the discussion assumes that the laser distance measurement is made in vacuum.

II. TFG PRINCIPLES OF OPERATION

Here we discuss the TFG, its architecture, its precision for incremental and absolute distance, and some recent improvements we have made. The TFG takes advantage of the convenience and effectiveness of shifting a laser wavelength to lock it to an interferometer fringe. The shift is converted to a radio frequency, which facilitates measurement to ample accuracy. In its original form, the TFG measured only incremental distance, the change of distance from the starting position, over a very limited range. A gauge that measures absolute distance determines the starting position as well, usually with less precision and with some bias. We have added "fringe hopping" to the TFG to extend the incremental measurement to an arbitrarily large range. This addition also gives it the capability to measure absolute distance.

Consider the measurement cavity in Fig. 1, or a nonresonant interferometer with the same optical path difference (OPD). It will have a series of intensity extrema (fringes) separated in frequency by the free spectral range

$$\Phi_0 = \frac{c}{2L_0}, \tag{1}$$

where L_0 is the measurement interferometer length. For a particular fringe, N, we have

$$N\lambda_0 = 2L_0. \tag{2}$$

(The N fringes could in principle be counted by moving the endpoints together.) For a slightly different length L, with the optical wavelength λ adjusted to stay on the same extremum,

$$N\lambda = 2L. \tag{3}$$

Let f_0 and f correspond to λ_0 and λ, respectively, $\delta L = L - L_0$, $\delta\lambda = \lambda - \lambda_0$ and $\delta f = f - f_0$. Then, during a period of smooth operation, with the wavelength locked to an extremum (i.e., N fixed)

$$\frac{\delta L}{L_0} = \frac{\delta\lambda}{\lambda_0} = \frac{-\delta f}{f_0 + \delta f},$$

$$\delta L = -\frac{\lambda_0}{2}\frac{\delta f}{\Phi_0 + \frac{\delta f}{N}} \approx -\frac{\lambda_0}{2}\frac{\delta f}{\Phi_0}. \tag{4}$$

Thus, the change of frequency measures the change of length.

A. Present implementation.

In our implementation of the TFG, we employ Pound–Drever–Hall locking. The current version is shown schematically in Fig. 1. An optical signal from the variable frequency source (VFS) of an adjustable wavelength λ_{VFS} is phase modulated at a frequency f_m and introduced into the measurement interferometer whose length, L, is to be determined. When λ_{VFS} is away from λ, the wavelength at the intensity extremum, the optical signal emerging from the interferometer is amplitude modulated, resulting in an electrical signal at the detector output at f_m with a magnitude and sign that indicate the offset. Synchronous detection at f_m and filtering yield a signal that is used to control λ_{VFS}, driving it back to λ. The corresponding optical frequency shift is measured by a frequency counter.

In any TFG realization, there is a limit, $\Delta f = \eta f_0$, to the range of optical frequency shift available for measuring incremental distance. This, in turn, sets the limit to the distance change that the laser gauge can follow smoothly

$$L_s = \frac{\Delta f}{\Phi_0}\frac{\lambda}{2} = \eta L = \frac{\Delta f}{1\ \mathrm{GHz}}\frac{L}{1\ \mathrm{m}}\frac{\lambda}{1\ \mu\mathrm{m}}3.3\ \mu\mathrm{m}. \tag{5}$$

For many purposes, L_S is inadequate. To overcome this limitation, we have built a controller with a nonlinear aspect such that when δf reaches the limit of the available range, a "hop" is introduced. Thus, for example, when the TFG controller reaches the low frequency threshold, it increases the optical frequency abruptly by an integer multiple (K) of Φ_0, so that the interferometer jumps from one null to another. If the hop is faster than the closed-loop response time, it will go "unnoticed," and yield minimal disruption. Similarly, the magnitude of the hop should be accurate so that the perturbation

of the TFG servo loop is small and thus damped quickly. After the hop, N has been replaced by $N+K$.

B. Slew rate

The "slew rate" of the TFG, i.e., the velocity that it can follow without slipping a fringe, depends on the minimum time between hops and the distance change corresponding to one hop. We have demonstrated hopping at 20 μs intervals without slipping fringes. The distance change for one hop is proportional to Δf, and inversely proportional to Φ, so proportional to L. Let t_h be the time between hops; the velocity is

$$v_s = \frac{\lambda}{1\ \mu\text{m}} \frac{\Delta f}{1\ \text{GHz}} \frac{L}{1\ \text{m}} \frac{10\ \mu\text{s}}{t_h} \left(0.33 \frac{\text{m}}{\text{s}}\right). \tag{6}$$

Note that measurement accuracy will suffer near this rate. For precision measurements, the servo must have more settling time. The present servo has a bandwidth of 50 kHz, implying a time constant $\sim 3\ \mu$s. To settle with the present TFG after a hop to within 1 pm, assuming a $\lambda/20$ transient, requires $t_h \gtrsim 35\ \mu$s. This corresponds to a slew rate of 0.01 m/s($L=0.5$ m, $\delta f = 300$ MHz, $\lambda = 633$ nm). Allowing measurement time while at high precision would require slewing at a lower rate.

C. Absolute distance

Because the TFG uses an adjustable optical frequency to measure incremental distance, the above-described hops are intrinsic to measuring distance changes of more than ηL, and little or no additional hardware is required for measuring absolute distance. By measuring the frequency shift δf before and after a hop, the TFG measures the free spectral range, Φ, of the measurement interferometer corresponding to the current length L. The estimate of L is then $c/(2\Phi)$. For the case of a dispersive medium in the path, see the Appendix. A few years ago, when we added hopping to the TFG, we demonstrated this capability to low accuracy (0.1 mm) in a preliminary test plagued by technical noise. We anticipate demonstrating a substantial improvement in this capability by using the refined TFG described in Sec. IV.

D. Statistical error

Here we calculate the random portion of the error in determining δL. We will not treat the error due to laser wavelength variation in any detail here. It affects our present TFG implementation in the same way it affects other laser gauges. Also, in many applications, the object is to measure or control the ratios of distances. In these cases, the impact of instability or error in the reference wavelength is eliminated or substantially reduced. We calculate the error assuming that λ_0 is known and stable. Consider small changes in $\delta f, \Phi$, and N. Proceeding from Eq. (4), keeping only leading terms in $\delta f/f$,

$$d(\delta L) = -\frac{\lambda}{2\Phi}\left(d(\delta f) - \frac{\delta f}{\Phi} d\Phi + \frac{(\delta f)^2}{\Phi}\frac{1}{N^2} dN\right). \tag{7}$$

Assuming that the errors in f, Φ, and N are uncorrelated, there are three terms in the error of δL, whose root sum square is the net error. Let $\sigma_\tau(\delta f)$ be the uncertainty of an estimate of δf based on data spanning a time τ. Then these terms are

$$\sigma_1 = \frac{\lambda}{2\Phi}\sigma_\tau(\delta f),$$

$$\sigma_2 = \frac{\lambda}{2\Phi}\frac{\delta f \sigma(\Phi)}{\Phi}, \tag{8}$$

$$\sigma_3 = \frac{\lambda}{2\Phi}\frac{(\delta f)^2}{\Phi}\frac{\sigma(N)}{N^2}.$$

Strictly speaking, the last line is valid only when $\sigma(N) \gg 1$; if not, N should be treated as a discrete variable and the expression replaced by one based on a discrete probability distribution. However, σ_3 can be ignored entirely for any plausible TFG. To see this, we combine Eqs. (1) and (2) and differentiate to get

$$\frac{\sigma(N)}{N} = \frac{\sigma(\Phi)}{\Phi} \tag{9}$$

and combine this with Eq. (8) to find

$$\sigma_3 = \frac{\delta f}{f}\sigma_2 \ll \sigma_2. \tag{10}$$

We next consider the importance of σ_2. Suppose that the TFG measures the frequency shifts, δf_1 and δf_2, before and after a hop of K fringes, where we choose K to be as large as possible, given the available range Δf. Then

$$\Phi = \frac{\delta f_2 - \delta f_1}{K}. \tag{11}$$

As long as undetected fringe hops are rare, we may use data taken over a span $T \gg \tau$ to form the estimates of δf_1 and δf_2, and

$$\sigma_T(\Phi) = \frac{2}{K}\sqrt{\frac{\tau}{T}}\sigma_\tau(\delta f). \tag{12}$$

Putting this result into Eq. (8) yields

$$\sigma_2 = 2\frac{\delta f}{K\Phi}\sqrt{\frac{\tau}{T}}\sigma_1. \tag{13}$$

Therefore, since $|\delta f| \lesssim K\Phi/2, \sigma_2 \ll \sigma_1$. Neglecting σ_2 and σ_3, the TFG's precision for incremental distance in a time τ is

$$\sigma_\tau(\delta L) = \frac{\sigma_\tau(\delta f)}{\Phi}\frac{\lambda}{2}. \tag{14}$$

How does $\sigma(\delta L)$ depend on L? If in time τ the frequency shift δf is determined to within a fraction α_τ of the full width at half maximum (FWHM) of the measurement interferometer fringe, the precision is

$$\sigma_\tau(\delta L) = \alpha_\tau \rho \frac{\lambda}{2}, \tag{15}$$

where ρ is the ratio of FWHM to Φ. For a nonresonant interferometer, $\rho = 0.5$, and for a cavity, $\rho = 1/\text{FINESSE}$. The shot-noise-limited sensitivity has been calculated for nonresonant[17] and resonant interferometers. For the present

TFG at $\lambda = 633$ nm, with $\sigma(\delta L) = 10$ pm in 0.1 s and finesse of 6.5, $\alpha_\tau = 2.1 \times 10^{-4}$. In the absence of technical noise, this would require $\sim 2 \times 10^7$ detected photons/s, or $\sim 7 \times 10^{-12}$ W of detected laser light.

With a nonresonant measurement interferometer, or a cavity with losses held constant as L varies, ρ is constant. Under the assumption that the precision of δf is a constant fraction of the linewidth, the TFG's incremental distance precision is independent of the length measured.

To calculate the error in absolute distance, again suppose that the frequency shifts δf_1 and δf_2 before and after a hop of K fringes are estimated using data spanning a time τ at each frequency. From Eq. (4)

$$\sigma_\tau(\delta f_i) = \frac{f}{L}\sigma_\tau(\delta L), \quad i = \{1,2\}. \tag{16}$$

Combining with Eq. (12) (setting $T = \tau$), one obtains an estimate of absolute distance L with uncertainty

$$\sigma_\tau(L) = \frac{L}{\Phi}\sigma_\tau(\Phi) = \frac{2f}{K\Phi}\sigma_\tau(\delta L) \geqslant \frac{2f}{\Delta f}\sigma_\tau(\delta L) = \frac{2}{\eta}\sigma_\tau(\delta L) \tag{17}$$

In the above equation, we assume that the errors in the two frequency measurements are uncorrelated. Since $\eta \ll 1$, the uncertainty in absolute distance must be much larger than the uncertainty in incremental distance when a comparable amount of time is used for each measurement. However, in many cases, absolute distance can benefit from a much longer averaging interval than incremental distance. A potential further improvement in absolute distance precision comes from the use of an increased bandwidth. In Eq. (17), Δf is the range for smooth operation. However, using the scheme for absolute distance described below for the SL-TFG, it is possible to have $K\Phi/\Delta f \gg 1$.

Additional statistical error comes from distance fluctuations due to vibration, turbulence, etc. In most cases, the Allan deviation (see below) of these fluctuations falls with increasing frequency. Thus, rapid hopping is advantageous up to the rate at which the servo settling time significantly decreases the time available for the separate measurements of δf_i.

Equation (17) implies that, under the (previously noted) assumption that the precision of δf is a constant fraction of the linewidth, the TFG's absolute distance precision is independent of the length measured, as for incremental distance. The greater difficulty of deducing absolute distance from Φ as L increases is compensated by the fact that a given frequency shift range Δf spans a greater number of fringes.

When the highest precision absolute distance is needed, it may be obtained by connecting to the incremental-precision scale. If the absolute precision is sufficient to determine the integer N, then a new and very precise absolute distance is

$$L = N\lambda + \delta L. \tag{18}$$

To make a reliable determination of N, we require $\sigma(L) < \lambda/\gamma$, where γ is at least 6. Using Eqs. (15) and (17), and assuming that all of the available frequency shift range is used for measuring absolute distance, this is equivalent to

$$\alpha < \frac{\sqrt{2}}{\gamma}\frac{\eta}{\rho}. \tag{19}$$

For the current TFG, this requires $\alpha < 1.6 \times 10^{-6}$, a two order of magnitude improvement. However, the SL-TFG is expected to meet this criterion (see Sec. IV A). If there is dispersion in the measurement interferometer, absolute distance can still be estimated as long as the dispersion is adequately modeled (see Appendix). If the dispersion is only due to the wavelength dependence of the phase change upon reflection, it may cause a small error in N, but will not prevent returning to the same value of N after an interruption. Furthermore, mirrors developed for use with femtosecond optical pulses, which reduce this variation, may make negligible the bias in the estimate of N.

III. REALIZATION AND TEST RESULTS

In our present implementation (Fig. 1), the VFS comprises a Zeeman-stabilized HeNe laser ($\delta\lambda/\lambda < 1 \times 10^{-11}$, 1 s; 2×10^{-11}, 1 min; 1×10^{-10}, 1 day), an acousto-optic deflector-modulator (ADM) driven by a voltage-controlled oscillator (VCO) operating over the range 187.5–312.5 MHz, and an electro-optic modulator (EOM) operating at $f_m = 8$ MHz. The free-space beam from the laser passes through the ADM four times, canceling the angular deflection and producing an optical frequency range $\Delta f = 500$ MHz. The EOM phase modulates the frequency-shifted laser signal with a modulation index of 1.5.

The phase modulator can produce a small direction variation at f_m, which can introduce error. To suppress this error, the beam is coupled into a single-mode polarization-maintaining fiber after exiting the phase modulator. The beam emerging from this "cleanup fiber" has no direction modulation, although, in principle, the variation of input coupling efficiency with beam direction produces some spurious amplitue modulation (AM) (Sec. III A). The fiber also serves to bring the beam to the measurement interferometer without requiring a rigid mechanical connection between the VFS and the interferometer. The cleanup fiber may be quite long, providing flexibility in the placement of the VFS. (We have used a length of ~ 10 m.) The fiber ends are cleaved at $\sim 8°$ to suppress reflections that would otherwise produce spurious AM. The beam emerging from the fiber is collimated and introduced into the measurement interferometer.

In the ADM, a traveling sound field diffracts the beam, and the diffraction efficiency into the desired order varies with δf. This intensity variation causes the servo's loop gain to vary correspondingly, which can cause error. The intensity variation is reduced with a "noise eater" circuit. A sample of the beam following the EOM is detected and fed back to the intensity modulation input of the VCO that drives the ADM. The ADM drive is set below saturation, so that reducing the drive reduces the diffraction efficiency.

A rf photodetector in the exit beam of the interferometer provides the error signal, which is amplified and detected synchronously by a mixer. The detected signal is further amplified and integrated by the loop controller and fed back to the VFS, which keeps the optical frequency centered on the

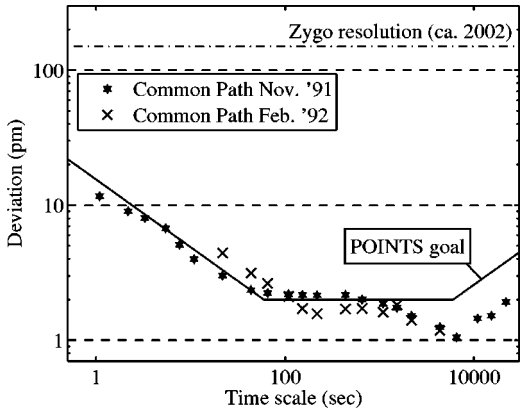

FIG. 2. Root Allan variance, $\overline{z}$, vs averaging time τ [Eq. (20)]. The TFG measured a path stabilized by the AFNG. They employed the same path in the measurement interferometer and HeNe laser, but different interferometer orders. The two runs shown used different approaches to the problem of spurious AM generated in the cleanup fiber. The Feb. 1992 run employed angled cleaves at the fiber ends, which is now a standard approach in the telecommunications industry.

interferometer null. The frequency shift may be read accurately using a frequency counter, or more rapidly by examining the voltage input to the VCO.

A. Statistical error

We have tested the TFG by comparing it with a gauge operating on a different principle, the alternating frequency null gauge (AFNG). The comparison was conducted with a nonresonant measurement interferometer employing open cornercube retroreflectors with front-surface overcoated aluminized mirrors, and operating in air. The AFNG drove a piezoelectric element to stabilize the interferometer OPD to the wavelength of the HeNe laser. Disturbances were dominated by turbulence of the air in the path. The TFG was locked to a neighboring interferometer fringe. Variations in the TFG output, $y(t)$, were due to TFG error, AFNG error, and imperfect removal of air-path fluctuations due to the finite gain of the loop comprising the AFNG and the piezoelectric actuator. The Allan deviation of the difference is defined as[18]

$$\overline{z}(\tau) = \left[\frac{1}{2(N-1)} \sum_{i=1}^{N-1} (y_{i+1} - y_i)^2 \right]^{1/2}, \tag{20}$$

where

$$y_i = \frac{1}{\tau} \int_{(i-1)\tau}^{i\tau} y(t)dt \tag{21}$$

and $y(t)$ is inferred from measurements of the VCO output frequency. $\overline{z}(\tau)$ is shown in Fig. 2. We reduced the deviation to meet the requirement of the POINTS project[19,20] for which the TFG was being developed.

Recently, we also tested the TFG's stability in a resonant optical cavity. This test was performed in vacuum, using a measurement interferometer formed by the two corner cube endpoints of the principle of equivalence measurement (POEM).[21] In these tests, the noise was not fully characterized, and showed some variation. The cavity length was $\sim 1/2$ m, and the Allan deviation was 10 pm for averaging times of 0.1–1 s during the quieter periods of operation. This is slightly better than the results at $\tau = 1$ s in Fig. 2, obtained over a decade ago. Figure 2 shows the difference of measurements made with respect to the same laser wavelength. The difference was thus insensitive to wavelength variations. The recent measurements were not differential, and if the laser wavelength varied at the level specified by the laser's manufacturer, it would have contributed significantly to the recently measured apparent distance variations.

B. Systematic error sources

Laser gauges can easily achieve great precision with modest laser power and integration time. As usual, connecting this to accuracy is more difficult. Here we discuss errors due to spurious AM from several sources, polarization-dependent phase shifts from mirrors at nonnormal incidence, refractive index variations, and beam alignment variations. Error sources are discussed again in the next section in connection with the SL-TFG.

1. Spurious AM

Consider points A and B along the nominal path from source to detector, and a spurious path by which light can get from A to B by traveling an extra distance (e.g., by making an extra round trip between partly reflecting surfaces or fiber ends, or scattering out of the beam, reflecting from a nearby surface, and scattering back in). The light traveling the spurious path interferes with the desired light and the net intensity is a function of wavelength. If the spurious path comes after the phase modulator, it converts part of the phase modulation sidebands into amplitude modulation in the same way that the measurement interferometer does, and so generates a spurious signal. Further, that signal will vary with wavelength and with any changes in the extra path length (e.g., induced by temperature, gas pressure, and mechanical stress on a fiber).

The simplest cure would be to avoid partly reflecting components after the phase modulator. This is not entirely possible due to reflections from the cleanup fiber ends. However, in the present TFG, we have succeeded in employing a cleanup fiber and achieving 2 pm accuracy by using angle-cleaved fiber ends. If this technique does not suppress spurious reflections enough for a particular objective, a servo can be employed in which the AM is sensed and corrected by feedback. This is similar to the noise eater described above, but suppresses amplitude fluctuations at f_m. A feedforward technique may also be used.

Another source of spurious AM is beam direction variation introduced by the phase modulator. The modulator in the present TFG is a Conoptics[22] model 370, configured for use as a phase modulator. It employs two crystals of ammonium dihydrogen phosphate (ADP). With z along the axis of fourfold symmetry, the electric field at f_m is applied along x, and propagation is along (0,1,1). In principle, the arrangement of the two crystals cancels the beam deflection, both the static deflection and that due to the electric field. Following the phase modulator, the beam is coupled to the cleanup fiber. Misalignments will arise from air currents, thermal distortions, or a residual variation of beam angle due to the optical

frequency shifter based on the ADM. These misalignments combine with the residual direction variations at f_m due to the EO modulator to cause AM. (These misalignments would be largely eliminated if the beam traveled to the phase modulator in fiber, instead of in free space.)

2. Polarization effects

When corner cubes are employed as end points for the measurement interferometer, the beam impinges on the reflectors at nonnormal incidence angles, typically greater than 45°. The phase change on reflection from a single surface experienced by signals in *s* and *p* polarizations can differ by as much as 30°, corresponding to a distance change of $\lambda/24$. Thus, even small variations in the polarization state would cause unacceptable variations in the apparent distance. This problem occurs in any laser gauge that uses cornercube retroreflectors. However, the TFG has two advantages in mitigating polarization errors: it may employ any chosen polarization in the measurement interferometer, and it may employ a resonant interferometer. For tests to date, we have placed a linear polarizer between the fiber output and the measurement interferometer, holding the polarization state constant. In a nonresonant interferometer, it might be better to employ a polarization state corresponding to an extremum of the distance, making the response to small polarization variations second order.

With a resonant interferometer, we rotated the polarization angle and found modes at two distinct optical frequencies. We selected one mode by setting the polarization angle to minimize the other. The ideal solution would be to employ a polarization eigenmode, which in practice may not be linearly polarized. The suppression of polarization error is enhanced over that in a nonresonant interferometer both because coupling of the polarized input beam to the undesired mode is suppressed, and because the eigenmodes are at different optical frequencies, so that the excitation of the suppressed mode causes little bias. The controller locks to the chosen mode. Peck[23] and others have studied the polarization eigenmodes of a cavity, and polarization effects of corner cubes.

Refractive index variation in the measurement interferometer affects all distance gauges in the same way. In our present setup, the retroreflectors are solid and each introduces 3.5 cm of glass path. In addition, the beamsplitter and a compensator plate are both in the measurement path. However, the measurement interferometer for the TFG can be a resonant cavity with an optical path entirely in vacuum, eliminating error from refractive index variations. Such an approach requires an alternative retroreflector design as well as injecting and extracting the light through a retroreflector surface that is partially transmitting. A retroreflector requiring substantially less path in glass is the cat's-eye,[24] which also has little effect on polarization.

All-reflective cornercube retroreflectors have no glass in the path, but existing designs may not have adequate dimensional stability. A "hollow-solid" all-reflective corner cube having the dimensional stability of a filled corner cube may be constructed. Looking into a corner cube retroreflector, one sees six sectors bounded by the (radial) lines between reflecting faces and their images. For a hollow-solid retroreflector, the beam must underfill these sectors. To construct such a retroreflector, one could start with a filled retroreflector, and remove the glass along the beam paths. To replace the reflecting function that has been cut away, front-surface reflectors would be attached to what had been the reflecting faces of the filled retroreflector. One or more of the attached reflectors could be made partially reflecting for coupling.

3. Alignment

A significant source of measurement error with any high precision distance gauge is beam alignment in the measurement interferometer. With $L=1$ m, a beam misalignment of 1.4 μrad gives an error of 1 pm, assuming that the beam started in perfect alignment. If a resonant cavity can be used for the measurement interferometer, misalignments must couple to off-axis modes, which are suppressed. Further, a powerful method is available for determining and maintaining alignment.[25] It is based on an optically stable resonator, which requires the resonator to include some focusing power. This is often done by making one cavity end mirror curved. Additional signals are injected into the cavity at the frequencies of the first off-axis modes. These are detected by a rf quadrant photodiode, are demodulated, and drive actuators to minimize the excitation of the off-axis modes, thus maintaining alignment. Sampas and Anderson demonstrated alignment sensitivity of 0.1 nrad/$\sqrt{\text{Hz}}$ from ~1 Hz to 1 kHz. A simpler approach, not requiring the added modulation, is to use dc quadrant photodiodes to provide the alignment signal. This method functions in a nonresonant interferometer as well, although error is further reduced in the resonant cavity by the passive suppression of off-axis modes.

IV. MORE ROBUST VERSION

We are developing a version of the laser gauge on which a spaceworthy instrument could be based. In this version of the TFG, we replace the HeNe laser with a tunable semiconductor source, and eliminate both the ADM and most of the free-space path in the VFS. When testing in laboratory air, this will reduce the influence of turbulence. When operating either in air or vacuum, eliminating free-space path will reduce error due to thermally driven movement of components. Fiber-coupled components also will keep the VFS modular, simplifying setup, reconfiguration, and repair. For a flight version, however, it may be desirable to eliminate the fiber connectors, employing fusion splicing instead.

In the SL-TFG, one laser (Tunable Laser in Fig. 3) will have its wavelength locked to the measurement interferometer. A second laser (Reference Laser) will be locked to a high-stability reference cavity, and the frequency difference (beat note) counted. A change of beat note indicates a change in *L*. The tunable laser's frequency control input is an analog signal that can be read faster, but with lower accuracy.

The SL-TFG will be based on distributed feedback (DFB) semiconductor diode lasers operating in the 1550 nm (190 THz) band. These lasers are available at moderate cost from several vendors, create most of their output in a single longitudinal mode, have adequate coherence length

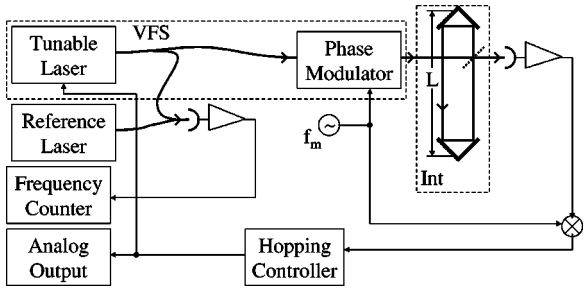

FIG. 3. Block diagram of the new tracking frequency gauge based on tunable semiconductor lasers and fiber-connected components. Int is measurement interferometer whose length, L, is to be measured. Digital output is *via* frequency counter. "Tunable Laser" and "Reference Laser" blocks may include filters for side-mode suppression.

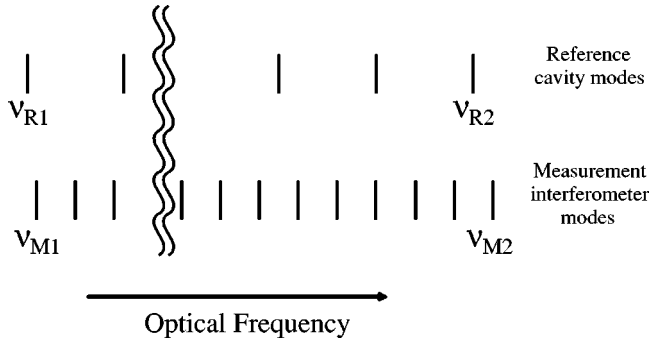

FIG. 4. Reference and measurement interferometer modes, for scheme in which a large range Δf_A of order 10 GHz is used for measurement of absolute distance, where Δf_A is larger than the detector or frequency counter bandwidth.

(~100 m), can be purchased with fiber-coupled output, and are rapidly tunable via their injection current. They have been used for atomic spectroscopy for more than a decade.[26]

For the SL-TFG, servo bandwidth higher than 100 kHz is a secondary goal. The intrinsic limit to servo bandwidth of the present TFG was a time delay in the ADM. In the SL-TFG, with a rapidly tuning DFB laser, the only intrinsic limit to bandwidth will be the light propagation time in the measurement interferometer. However, it will be necessary to address a complication posed by the frequency modulation (FM) response of DFB lasers. At low frequencies, the response is thermal, while at high frequencies ($\gtrsim$1 MHz), it is due to changes in carrier density. The two responses have the opposite sign. This problem has been solved for some diode laser sources.[27]

A. Error sources (SL-TFG)

The "side modes" of DFB lasers are a possible source of error. While most of the light is emitted in the principal longitudinal mode, some is emitted in other modes. For example, the JDS Uniphase CQF935 laser[22] has side modes at ~85 GHz spacing, extending >10 nm (1.2 THz) either side of the principal mode. Its specified side-mode suppression ratio (SMSR) is 30 dB min, 45 dB typical. For a nonresonant measurement interferometer operating at $\lambda = 1550$ nm and SMSR = 30 dB, the maximum error due to a side mode is 120 pm. This is mitigated by three factors. (1) The laser side modes have a broader spectral width than the principal mode. In many cases they span several measurement interferometer modes, and there is reduction by averaging. (2) If the measurement interferometer is optically resonant, the effect of side modes is suppressed by the finesse, since the side-mode linewidth will likely be greater than that of the measurement interferometer resonance. (3) If necessary, the side modes can be filtered out, e.g., by the JDS wavelength division multiplexing filters[22] that provide 50 dB in stop band suppression, reducing the error due to side modes by a factor 10^5.

For the SL-TFG, the analog of laser wavelength variation is a variation of the reference wavelength. If that wavelength is generated by stabilizing a laser to a cavity, the statistical component of its error can be reduced by using a two-mirror Fabry-Perot resonator of high finesse. In many applications, systematic error in the reference is not an important consideration (Sec. II D). If it is important, it can be reduced by making the reference cavity of thermally stable material and locating it in a thermally stable environment, or using instead an atomic line reference.

B. Absolute distance with SL-TFG

In Sec. II C, we described the scheme for measuring absolute distance with the present TFG. The SL-TFG will operate at ~1550 nm and could employ a frequency shift for absolute distance Δf_A of order 10 GHz $\gg \Delta f$. If it achieves 10 pm precision at the longer wavelength (implying a reduction of α in inverse proportion to the wavelength), it will meet the criterion [Eq. (19)] for connecting absolute distance with incremental.

The scheme illustrated in Fig. 4 allows the measurement of absolute distance based on a frequency shift of Δf_A. It permits the measurement of Δf_A without the need for wideband photodetectors or counters. By employing a variant of this scheme, it would be possible to measure absolute distance with just two lasers using bootstrap methods, provided that the measurement and reference interferometers are stable. However, we limit our discussion here to the approach using four lasers.

There would be two reference lasers at optical frequencies ν_{R1} and ν_{R2}, both locked to modes of the reference cavity that are separated by as large a frequency span Δf_A as possible, limited by the tuning range of the lasers. The first and second measurement lasers would be locked to measurement interferometer modes at frequencies ν_{M1} and ν_{M2}, near ν_{R1} and ν_{R2}, respectively. With the lasers locked this way, the frequency differences $\nu_{Mi} - \nu_{Ri}, i = 1, 2$, would be accurately known by counting beat notes. The quantity $\nu_{M2} - \nu_{M1} = [(\nu_{M2} - \nu_{R2}) - (\nu_{M1} - \nu_{R1}) + (\nu_{R2} - \nu_{R1})]$ would be a large integer multiple, K, of Φ.

To measure $\nu_{R2} - \nu_{R1}$, the first reference laser would remain locked to a reference cavity mode at ν_{R1}, and the second reference laser would start locked to a reference cavity mode near (e.g., adjacent to) the first, at a frequency difference within the range of the photodiode and frequency counter. The free spectral range of the reference cavity would be precisely determined, taking as much time as necessary. The second reference laser would then be hopped a known

number of reference cavity modes away, to lock to a mode at ν_{R2}. $\nu_{R2}-\nu_{R1}$ would now be known accurately, although at a frequency too high to count directly.

C. Alternative approach to absolute distance

A reviewer has pointed out that it has been proposed,[28] although not yet demonstrated, that a phase-stabilized femtosecond (fs) laser can be used for measuring absolute distance. The work is motivated by the convenience of a phase-stable pulse train, which allows time of flight and interferometric distance information to be collected with a single laser, thus providing a huge dynamic range in distance. Length ambiguity would be resolved by sweeping the pulse repetition rate. The SL-TFG provides the same dynamic range, measuring absolute distance by hopping. Initially, the hop is by a single order of the measurement interferometer, yielding a measurement with no distance ambiguity. Increased precision would be obtained by hopping over several orders. With both fs lasers and the SL-TFG, a transition could be made from the initial absolute distance measurement to one based on optical phase and a knowledge of the (integer) number of wavelengths in the measured path. It should be noted that the semiconductor DFB lasers used in the SL-TFG have significant advantages: they have benefited from a large volume of commercial development for telecommunications, and were designed for environments with similar requirements to those of a laser on a space-based astronomical instrument (except radiation). Also, the DFB lasers tune in about 1 ns, whereas in at least some implementations, fs lasers require tuning by changing a physical length. The higher speed of the DFB is convenient when a laser gauge must follow a rapidly changing distance, or when the readings are used in compensating for vibration.

ACKNOWLEDGMENTS

The authors gratefully acknowledge support from the National Aeronautics and Space Administration through Grant No. NNC04GB30G, the Smithsonian Institution, including its Scholarly Studies Program, and the Naval Research Laboratory, and the contributions of the following students: Kelzie Beebe, Jennifer Hoffman, Alejandro Jenkins, Brandon McKenna, and Glen Nixon.

APPENDIX: ABSOLUTE DISTANCE AND GROUP VELOCITY

Here we look in more detail at the measurement of absolute distance with the TFG and show that it is based on group delay. Consider a pair of adjacent orders of the interferometer, with a laser locked to each. Then, if $n=c/u$ is the refractive index along the measurement path and u is the corresponding (phase) velocity, the round-trip path is

$$2L = N\frac{2\pi c}{\omega n} = (N+1)\frac{2\pi c}{\omega_1 n_1}, \tag{A1}$$

where $\omega=2\pi c/\lambda$, λ is the free-space wavelength, $n_1=n+\Delta n$, $\omega_1=\omega+\Delta\omega$, $\Delta\omega=2\pi\Phi$, and Φ is the free spectral range defined in Eq. (1). Solving the above for N yields, to lowest order,

$$N \approx \frac{\omega}{\Delta\omega}\left(1-\frac{\omega}{n}\frac{\Delta n}{\Delta\omega}\right). \tag{A2}$$

By combining the above two equations, we obtain

$$L \approx \frac{1}{2}\frac{2\pi c}{\Delta\omega n}\left(1-\frac{\omega}{n}\frac{\Delta n}{\Delta\omega}\right) = \frac{\pi}{\Delta\omega}\left(u-\frac{\omega c}{n^2}\frac{dn}{d\lambda}\frac{d\lambda}{d\omega}\right). \tag{A3}$$

We can simplify the above by using

$$\frac{dn}{d\lambda} = -\frac{n^2}{c}\frac{du}{d\lambda}$$
$$\frac{d\lambda}{d\omega} = -\frac{2\pi c}{\omega^2} \tag{A4}$$

to obtain

$$L = \frac{1}{2\Phi}\left(u-\lambda\frac{du}{d\lambda}\right) = \frac{u_g}{2\Phi}, \tag{A5}$$

where u_g is the group velocity. (See, for example, Panofsky and Phillips[29] for a discussion of group delay.)

Although the above result is obtained in the TFG context, it is true in general that a laser gauge that measures absolute distance is finding group delay. There are two cases, although they are not substantially different. The electronic distance meters used in surveying send pulses of light and correlate the detected returned power with a replica of the pulse sequence delayed by a time t. The round-trip time modulo the "ambiguity length" is the value of t that yields the highest correlation. This is the traditional case of group delay. In other schemes, such as that analyzed above for the TFG, there is an explicit shift of frequency.

[1] K. C. Gendreau, W. Cash, and A. Shipley, Proc. SPIE **5168**, 420 (2003). See also http://maxim.gsfc.nasa.gov.
[2] K. G. Carpenter *et al.*, Proc. SPIE **4854**, 293 (2003). See also http://hires.gsfc.nasa.gov/~si.
[3] Y. Gursel, Proc. SPIE **3350**, 571 (1998), and references therein.
[4] C.-M. Wu, J. Lawall, and R. D. Deslattes, Appl. Opt. **38**, 4089 (1999).
[5] J. Lawall and E. Kessler, Rev. Sci. Instrum. **71**, 2669 (2000).
[6] P. G. Halverson and R. E. Spero, J. Opt. A, Pure Appl. Opt. **4**, S304 (2002).
[7] F. Zhao, R. Diaz, G. M. Kuan, N. Sigrist, Y. Beregovski, L. L. Ames, and K. Dutta, Proc. SPIE, **4852**, 370 (2003), and references therein.
[8] O. P. Lay, S. Dubovitsky, R. D. Peters, J. P. Burger, S.-W. Ahn, W. H. Steier, H. R. Fetterman, and Y. Chang, Opt. Lett. **28**, 890 (2003).
[9] H. Fang, A. Picard, and P. Juncar, Rev. Sci. Instrum. **73**, 1934 (2002).
[10] J. A. Stone and A. Stejskal, Metrologia **41**, 189 (2004).
[11] J. A. Stone *et al.*, Appl. Opt. **38**, 5981 (1999).
[12] C. M. Caves, Phys. Rev. Lett. **45**, 75 (1980).
[13] C. M. Caves, Phys. Rev. D **23**, 1693 (1981).
[14] K. Jacobs, I. Tittonen, H. M. Wiseman, and S. Schiller, Phys. Rev. A **60**, 538 (1999).
[15] M. C. Noecker, J. D. Phillips, R. W. Babcock, and R. D. Reasenberg, Proc. SPIE **1947**, 174 (1993).
[16] R. D. Reasenberg, J. D. Phillips, and M. C. Noecker, U.S. Patent No. 5,412,474 (2 May 1995).
[17] B. J. Meers and K. A. Strain, Phys. Rev. A **44**, 4693 (1991).
[18] D. W. Allan, Proc. IEEE **54**, 221 (1966). Note that the Allan variance as originally defined was for frequency measurements and included a normalization (i.e., $\Delta f/f$) that is not applicable here.
[19] R. D. Reasenberg *et al.*, Astron. J. **32**, 1731 (1988).

[20] R. D. Reasenberg *et al.*, Proc. SPIE **2807**, 32 (1996).
[21] R. D. Reasenberg and J. D. Phillips, Class. Quantum Grav. **18**, 2435 (2001).
[22] This information is for technical communication only and does not constitute an endorsement of these products.
[23] E. R. Peck, J. Opt. Soc. Am. **52**, 253 (1962).
[24] J. J. Snyder, Appl. Opt. **14**, 1825 (1975).
[25] N. M. Sampas and D. Z. Anderson, Appl. Opt., **29**, 394 (1990).
[26] C. E. Wieman and L. Hollberg, Rev. Sci. Instrum. **62**, 1 (1991).
[27] L. N. Langley, M. D. Elkin, C. Edge, M. J. Wale, U. Gliese, X. Huang, and A.J. Seeds, IEEE Trans. Microwave Theory Tech. **47**, 1257 (1999).
[28] J. Ye, Opt. Lett. **29**, 1153 (2004).
[29] W. K. Panofsky and M. Phillips, *Classical Electricity and Magnetism* (Addison–Wesley, Reading, MA, 1962), p. 202.